IEEE Access
Multidisciplinary ⋮ Rapid Review ⋮ Open Access Journal

Received November 14, 2019, accepted December 2, 2019, date of publication December 9, 2019, date of current version December 23, 2019.

Digital Object Identifier 10.1109/ACCESS.2019.2958414

A Novel Multi-Band Reduced Sampling Rate and I/Q Compensation Technique for RF Power Amplifiers

JINGMEI ZHAO[1,2], LINBO ZHAI[1], AND FENG YANG[1]
[1]School of Information Science and Engineering, Shandong Normal University, Jinan 250358, China
[2]Management Science and Engineering, Postdoctoral Research Station, Shandong Normal University, Jinan 250358, China

Corresponding author: Jingmei Zhao (jingmeizhao@126.com)

This work was supported in part by the Key Research and Development Program in Shandong Province of China under Grant 2017GGX10142, and in part by the Postdoctoral Start-Up Fund under Grant 195332.

ABSTRACT In this paper, a novel multi-band reduced sampling rate technique is proposed for power amplifier (PA) linearization system. It is used to enhance performance and reduce hardware costs in spectrum aggregation discontinuous broadband systems and compensate in-phase/quadrature (I/Q) imbalance in the multi-band case. During the feedback loop process of sampling rate, a band-limited filter is introduced, and the frequency band extrapolation is carried out so that the spectrum outside the limited band is compensated effectively. Theoretical analysis is performed to compare the proposed method and the conventional methods. To evaluate the performance of the proposed method, a broadband PA is excited by a tri-band signal composed of a 20 MHz long-term evolution (LTE) signal at 1.31 GHz, a 20 MHz 4-carrier wideband code division multiple access (WCDMA) signal at 2.49 GHz, and a 20 MHz 2-carrier WiMAX signal at 2.58 GHz respectively. The experimental results demonstrate that the normalized mean square error (NMSE) can get high accuracy less than −41 dB, with peak-to-average power ratio (PAPR) equaling 9 dB accompanied by a large reduction in sampling rate. Error vector magnitude (EVM) is 1% better than band-limited memory polynomial (MP) model and 2.3% better than conventional MP model.

INDEX TERMS Band limited, digital predistortion, I/Q imbalance, multi-band, power amplifier, sampling rate.

I. INTRODUCTION

With the rapid development of wireless communication technology, the signal bandwidth becomes wider to support higher data rate under the limited spectrum resources. Recently, dual-band power amplifier (PA) technology has greatly developed [1]. Meanwhile, the corresponding digital predistortion (DPD) also has great development, multi-band DPD is still a relatively new field. Currently non-continuous carrier aggregation (CA) is also widely used in today's wireless carrier. The significant challenges in these systems are high sampling rate and high cost.

The deployment and promotion of 5G will allow ultra-wideband signals to be transmitted across the hundreds of megahertz band in order to obtain the required high system capacity [2]–[4]. Because of the variety of spectrum regulation in different countries, it is difficult for a single operator to obtain continuous broadband spectrum, which leads to the common situation of frequency division. In order to achieve high data rate transmission and good spectral efficiency, CA technology [5]–[7] is widely used in system such as long-term evolution (LTE)-Advanced, and allows different communication signals to be transmitted in different frequency bands at the same time. Spectrum scarcity and ever-increasing data rate requirements are two major factors for carrier convergence in modern wireless communication systems.

Recently, several broadband DPD with low-sampling and tri-band DPD methods have been proposed [8]–[10]. Younes et al. extended the memory polynomial to three-dimensional [8], which is based on the analysis of crosstalk between the fundamental frequencies. However, the choice of center frequency will directly affect in-band inter-modulation distortion (IMD) and the unfilterable inter-band IMD. In [9],

The associate editor coordinating the review of this manuscript and approving it for publication was Zeeshan Kaleem.

T. Tian et al. proposed a concurrent tri-band DPD scheme based on dynamic deviation reduction (DDR) model, and the importance of out-of-band intermodulation components has been analyzed. Su et al. derived an even mode multi-band model and generalized to address IMD and cross-band modulation products located at the vicinity of the bands of interest [10]. In [11], authors proposed a concurrent transmitter hardware architecture with band-limited sources and a multiple-input multiple-output (MIMO) digital nonlinear mitigation technique with sub-band Volterra.

For the low sampling rate techniques, C. Yu et al. proposed a band limited predistortion model based on Volterra series and a predistortion method with controllable frequency components [12], [13]. For each basis function, a band limit function represented by a low-pass filter is introduced to ensure that the model bandwidth matches the PA output bandwidth. In order to achieve higher efficiency and reduce the spectrum acquisition range, the two methods sacrifice some linearity and retain some distortion in the output signal.

Mkadem et al. proposed multi-band complexity-reduced model algorithm for PA [14]. Guan et al. proposed a direct learning digital predistortion method for PA [15]. This method can reduce the sampling rate requirement of the analog-to-digital converter (ADC) on the feedback path. A modified gauss-newton iterative equation is derived by using a single branch feedback signal at a low rate.

The In-phase/quadrature (I/Q) imbalance of the transmitter directly affects the performance of the linearized circuit of the PA which results in the urgency to eliminate I/Q imbalance in the digital base-band. At present, there are two main methods to correct I/Q imbalance. One is to adopt a high-performance simulator, and the other is to estimate and correct I/Q imbalance in the digital domain by digital signal processing method. In [16]–[18], a scheme of estimation and online positioning without pilot frequency was proposed to solve the problem of unbalanced frequency selection I/Q of multi-band and multi-standard of broadband direct frequency converter transmitter. Reference [19] eliminated the distortion caused by the frequency dependence imbalance between analog I channel and Q channel of direct conversion transmitter. Nassery et al. put forward a multi-step self-test technology that utilized self-mixing envelope detector to realize unbalanced and non-linear transmitter I/Q [20], and designed test signals with linear state expressions.

Gandhi et al. proposed novel digital signal processing algorithms for linearizing PAs and correcting RF impairments in multi-standard, multi-mode, and multi-band wireless communication transceiver platforms [21]. They introduced an integrated transmit and receive digital signal processing solution which provides compensation for key RF system chain impairments. In 2017, Khan et al. proposed joint effects of I/Q imbalance and PA distortion for RF MIMO transmitters in the presence of crosstalk [22]. This paper discussed candidate models for the DPD of static I/Q imbalanced sources exciting a dynamic MIMO Volterra system.

In this paper, we propose a novel multi-band digital predistortion, which can achieve significant improvement of linearization property and reduce the sampling rate in the feed-back loop. The new I/Q compensation method is applied to the proposed multi-band DPD system. Meanwhile, without sacrificing the linearity and efficiency, both theoretical analysis and experimental results show that the non-continuous and aggregated carrier system can benefit a lot from it.

The remainder of this paper is organized as follows. In Section II, the tri-band model and band limited model are briefly introduced. In Section III, the proposed DPD architecture and multi-band limited extension (MBLE) model algorithm based on new gauss-seidel will be described in detail. Several interesting test cases along with experimental results are presented in Section IV and Section V. The conclusion is given in Section VI.

II. MODEL PREMISE

A. TRI-BAND MODEL

If the multi-band system has three bands, the input signal can be given as equation (1).

$$x(t) = x_1(t) + x_2(t) + x_3(t) \tag{1}$$

where $x_i(t)$ $(i = 1, 2, 3)$ presents the band i input signal and centered at the corresponding the three RF frequencies f_i. The complex envelope of the pass-band signal $x_i(t)$ at the angular frequency $\omega_i = 2\pi f_i$ is given as:

$$x_i(t) = \frac{\tilde{x}_i(t)e^{j\omega_i t} + \tilde{x}_i^*(t)e^{-j\omega_i t}}{2} \tag{2}$$

Using the binomial expansion and grouping all the elements that lie around different frequencies, the results are shown as

$$\begin{aligned} y = &\sum_{k=1}^{N}\sum_{r_1=0}^{k}\sum_{r_2=0}^{r_1}\sum_{k_2=0}^{k-r_1}\sum_{k_3=0}^{r_2}\sum_{k_4=0}^{r_1-r_2}\frac{1}{2^k}a_k C_{r_1}^{k} C_{r_2}^{r_1} C_{k_2}^{k-r_1} C_{k_3}^{r_2} C_{k_4}^{r_1-r_2} \\ &\times([\tilde{x}_1|\tilde{x}_1|^{2k_2}|\tilde{x}_2|^{2k_3}|\tilde{x}_3|^{2k_4}]^{e^{j\omega_1 t}} \\ &+[\tilde{x}_2|\tilde{x}_1|^{2k_2}|\tilde{x}_2|^{2k_3}|\tilde{x}_3|^{2k_4}]^{e^{j\omega_2 t}} \\ &+[\tilde{x}_3|\tilde{x}_1|^{2k_2}|\tilde{x}_2|^{2k_3}|\tilde{x}_3|^{2k_4}]^{e^{j\omega_3 t}} \\ &+[\tilde{x}_1^*\tilde{x}_2^2|\tilde{x}_1|^{2(k_2-1)}|\tilde{x}_2|^{2k_3}|\tilde{x}_3|^{2k_4}]^{e^{j(2\omega_2-\omega_1)t}} \\ &+[\tilde{x}_1^2\tilde{x}_2^*|\tilde{x}_1|^{2k_2}|\tilde{x}_2|^{2(k_3-1)}|\tilde{x}_3|^{2k_4}]^{e^{j(2\omega_1-\omega_2)t}} \\ &+[\tilde{x}_2^2\tilde{x}_3^*|\tilde{x}_1|^{2k_2}|\tilde{x}_2|^{2k_3}|\tilde{x}_3|^{2(k_4-1)}]^{e^{j(2\omega_2-\omega_3)t}} \\ &+[\tilde{x}_2^*\tilde{x}_3^2|\tilde{x}_1|^{2k_2}|\tilde{x}_2|^{2(k_3-1)}|\tilde{x}_3|^{2k_4}]^{e^{j(2\omega_3-\omega_2)t}} \\ &+[\tilde{x}_1\tilde{x}_2^*\tilde{x}_3|\tilde{x}_1|^{2k_2}|\tilde{x}_2|^{2(k_3-1)}|\tilde{x}_3|^{2k_4}]^{e^{j(\omega_1+\omega_3-\omega_2)t}} + \cdots) \end{aligned} \tag{3}$$

From (3), it can be seen that, in addition to the fundamental frequency products, $2\omega_2 - \omega_1$, $2\omega_1 - \omega_2$ and other cross-modulation products are also included. In the binomial expansion, we can only take the components away from the fundamental frequency, and other harmonic and cross modulation components should not be considered because they are far from the effective signal and can be filtered out.

B. BAND-LIMITED MODELING

The band limiting function is inserted into each valid output signal, and the appropriate form transformation is made to obtain the new DPD model, as shown in the following equation

$$
\begin{aligned}
&y_{BL1}(n)\\
&=\sum_{m=0}^{M}\sum_{k=0}^{K}\sum_{g=0}^{k}\sum_{c=0}^{g} h_{mkgc,BL1}[x_{BL1}(n-m)|x_{BL1}(n-m)|^{k-g}\\
&\quad\times|x_{BL2}(n-m)|^{g-c}|x_{BL3}(n-m)|^{c} * b_1(n)]\\
&=\sum_{m=0}^{M}\sum_{k=0}^{K}\sum_{g=0}^{k}\sum_{c=0}^{g} h_{mkgc,BL1}\{\sum_{l=0}^{L}[x_{BL1}(n-m-l)\\
&\quad\times|x_{BL1}(n-m-l)|^{k-g}|x_{BL2}(n-m-l)|^{g-c}\\
&\quad\times|x_{BL3}(n-m-l)|^{c}b_1(l)]\}
\end{aligned}\tag{4}
$$

$$
\begin{aligned}
&y_{BL2}(n)\\
&=\sum_{m=0}^{M}\sum_{k=0}^{K}\sum_{g=0}^{k}\sum_{c=0}^{g} h_{mkgc,BL2}[x_{BL2}(n-m)|x_{BL1}(n-m)|^{k-g}\\
&\quad\times|x_{BL2}(n-m)|^{g-c}|x_{BL3}(n-m)|^{c} * b_2(n)]\\
&=\sum_{m=0}^{M}\sum_{k=0}^{K}\sum_{g=0}^{k}\sum_{c=0}^{g} h_{mkgc,BL2}\\
&\quad\times\{\sum_{l=0}^{L}[x_{BL2}(n-m-l)|x_{BL1}(n-m-l)|^{k-g}\\
&\quad\times|x_{BL2}(n-m-l)|^{g-c}|x_{BL3}(n-m-l)|^{c}b_2(l)]\}
\end{aligned}\tag{5}
$$

$$
\begin{aligned}
&y_{BL3}(n)\\
&=\sum_{m=0}^{M}\sum_{k=0}^{K}\sum_{g=0}^{k}\sum_{c=0}^{g} h_{mkgc,BL3}\times[x_{BL3}(n-m)|x_{BL1}(n-m)|^{k-g}\\
&\quad\times|x_{BL2}(n-m)|^{g-c}|x_{BL3}(n-m)|^{c} * b_3(n)]\\
&=\sum_{m=0}^{M}\sum_{k=0}^{K}\sum_{g=0}^{k}\sum_{c=0}^{g} h_{mkgc,BL3}\{\sum_{l=0}^{L}[x_{BL3}(n-m-l)\\
&\quad\times|x_{BL1}(n-m-l)|^{k-g}|x_{BL2}(n-m-l)|^{g-c}\\
&\quad\times|x_{BL3}(n-m-l)|^{c}b_3(l)]\}
\end{aligned}\tag{6}
$$

where $*$ represents the convolution, $h_{mkgc,BLi}$ $(i = 1, 2, 3)$ are band-limited complex Volterra kernel of the band-limited model, and b_i $(i = 1, 2, 3)$ are the band-limiting function of the three bands, which are used to match the bandwidth of the captured signal. The band-limiting function can be implemented with a linear filter. The effective bandwidth can be selected according to the output bandwidth requirements of the system and designed in advance in the frequency domain. The Least Squares (LS) solutions of (4)-(6) are

$$
\mathbf{h}_{BLi} = \left(\mathbf{X}_{BLi}^{\mathrm{H}}\mathbf{X}_{BLi}\right)^{-1}\mathbf{X}_{BLi}^{\mathrm{H}}\mathbf{Y}_{BLi} \tag{7}
$$

where $(\cdot)^{\mathrm{H}}$ and $(\cdot)^{-1}$ denote the conjugate transpose and the inverse matrix respectively, $\mathbf{h}_{BLi}$ are the coefficient matrix, $\mathbf{X}_{BLi}$ are matrixes of band-limited input signals, and $\mathbf{Y}_{BLi}$ are matrixes of output signals. Based on the above band-limited model, it is possible to compensate for the inside distortion of the filter's pass-band.

In order to get a wider linear range, the band-limited signal will be continuously processed in the subsequent modules. In this structure, the PA output can be arbitrarily selective linearized according to user's demand. The bands to be linearized can be determined by the corresponding band selection module. The proposed method can be applied to multi-band systems with large intervals.

To achieve more flexibility as well as lower complexity and cost, a linearization band selection technique for multi-band signals is obtained as

$$
\begin{aligned}
u(n) = {}& [x_1(n), x_2(n), x_3(n)] * d_1(n)\\
&+ [x_1(n), x_2(n), x_3(n)] * d_2(n)\\
&+ [x_1(n), x_2(n), x_3(n)] * d_3(n)
\end{aligned}\tag{8}
$$

where $d_1(n)$, $d_2(n)$ and $d_3(n)$ represent the band selection function for input signal. Band selection function can be realized by band-pass filter, corresponding to the frequency of each signal. The bands that need to be linearized can be selected by setting different $d_i(n)$ $(i = 1, 2, 3)$. If the feedback signal is incompleted, it will lead to the uncontrollable result that happens outside the obtained spectrum region. This will deteriorate the linearization performance of the RF frontend system.

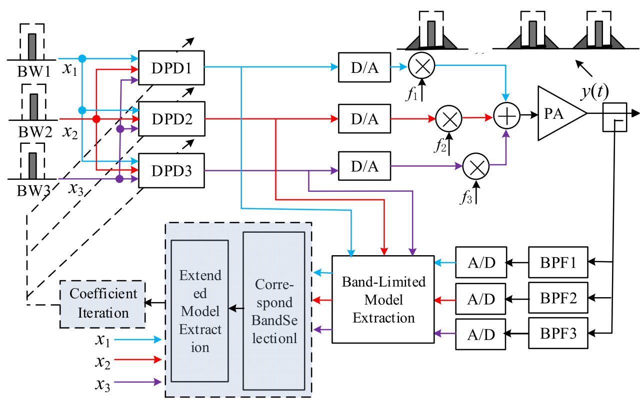

FIGURE 1. Block diagram of proposed tri-band predistortion system.

III. OUR PROPOSED STRUCTURE AND MULTI-BAND LIMITED EXTENSION MODEL

A. SYSTEM STRUCTURE

In CA system, three or more bands and the maximum frequency spacing are important factors to be considered in predistortion linearization. Take the tri-band linearization system as example, Fig. 1 shows the structure for proposed multi-band limited DPD algorithm with extended model iteration.

At the end of transmission, three input signals are up-converted to the corresponding frequency range, and low-pass filter functions are applied to limit their bandwidths. The band limited model is extracted with BPF in the feedback loop, and then the extracted coefficients are extended in full band by Gauss-Seidel algorithm.

B. EXTEND THE RANGE OF LINEARIZATION

In the case of tri-band, there are many out-of-band cross-modulation products, especially those located near the effective signal, which have to be alleviated because of their great influence on the quality of transmission. Considering the interference terms around the useful high-power signal, the whole tri-band model can be expressed as

$$y_i(n) = \sum_{i=1}^{3}[y_{BLi}(n) + y_i^E(n)] \tag{9}$$

where $y_{BLi}(n)$ $(i = 1, 2, 3)$ are the band-limited output signal given in (4)-(6). $y_i^E(n)$ are the out-of-band distortion components near the useful signal band, and can be derived as

$$y_i^E(n) = \sum_{m=1}^{M}\sum_{k=0}^{K}\sum_{g=0}^{k} x_i(n-m)|x_i(n-m)|^{k-g} \cdot \prod_{k=1}^{K} x_{L_k}(n-m) \times x^*_{T_k}(n-m)e^{j[\omega_i - \sum_{k=1}^{K}(\omega_{L_k} - \omega_{T_k})]} \tag{10}$$

where $i, L_k, T_k \in [1, 2, 3]$, $i \neq L_k$, $L_k \neq T_k$, the angular frequency is $\omega_i + \sum_{k=1}^{K}(\omega_{L_k} - \omega_{T_k})$. The high power level of sideband is an important reason for the obvious distortion effect. After getting band-limited results, the parameters $\mathbf{h}_{BLi}$ combining the full-band input signal $x_i(n)$ can achieve the full-band output signal which is obtained as follows

$$\mathbf{Y}_i = \mathbf{X}_i \cdot \mathbf{h}_i \tag{11}$$

where $\mathbf{Y_i}$ is the output signal matrix which is composed by the full-band output signal of $y_i(n)$, and $\mathbf{Y_i} = [y_i(0), y_i(1), \ldots, y_i(N-1)]^T$. $\mathbf{X}_i$ is the input signal matrix generated from the original full-band input signal $x_i(n)$. If the linearized bandwidth is required to be high, the distortion products outside the limited bandwidth should also be alleviated in the case of multi-band. The reason is that many out-of-band IMD would be located around the useful signal, and the DPD performance will be greatly affected.

In order to take the exact parameters under the multi-band case of the extended band range, the modified Gauss-Seidel method is applied in this paper. Firstly, $\mathbf{X}_i$ is split as $\mathbf{X}_i = \mathbf{A}_i - \mathbf{B}_i$, $(i = 1, 2, 3)$, $\mathbf{A}_i$ is non-singular matrix, and the basic iteration of (11) is

$$\mathbf{h}_i^{(k+1)} = \mathbf{A}_i^{-1}\mathbf{B}_i\mathbf{h}_i^{(k)} + \mathbf{A}_i^{-1}\mathbf{Y}_i \tag{12}$$

where $\mathbf{A}_i^{-1}\mathbf{B}_i$ is iterative matrix of (11), $(k = 0, 1, 2\ldots)$ representing the iteration number. Generally, the matrix $\mathbf{X}_i$ can also be decomposed into three matrices as $\mathbf{X}_i = \mathbf{D}_i - \mathbf{L}_i - \mathbf{U}_i$, where $\mathbf{D}_i$ is non-singular diagonal matrix, $\mathbf{L}_i$ and $\mathbf{U}_i$ represent lower triangular and upper triangular matrix respectively. If the condition number of the coefficient matrix is large, the matrix is ill-conditioned for solving the equation, and there will be slow convergence or even no convergence. The following preconditioning methods are proposed to improve the above problems. After being left-multiplied invertible matrix $\mathbf{P}_i$ at both ends, equation (11) is equivalently converted into preconditioned form as

$$\mathbf{P}_i\mathbf{Y}_i = \mathbf{P}_i\mathbf{X}_i \cdot \mathbf{h}_i \tag{13}$$

where $\mathbf{P}_i$ is the reversible pretreatment factor. In order to make the improved Gauss-Seidel method converge faster, we need to pre-select the pretreatment matrix $\mathbf{P}_i$. When the diagonal elements of $\mathbf{X}_i$ are simplified to 1, the expression of $\mathbf{P}$ can be expressed as follows.

$$\mathbf{P}_{\lambda\_i} = \mathbf{I} + \mathbf{S}_{\lambda\_i} = \begin{bmatrix} 1 & 0 & \cdots & 0 & 0 \\ -\lambda_2 x_{21} & 1 & \cdots & 0 & 0 \\ \vdots & \vdots & \cdots & \vdots & \vdots \\ -\lambda_{N-1}x_{N-1,1} & 0 & \cdots & 1 & 0 \\ -\lambda_N x_{N,1} & 0 & \cdots & 0 & 1 \end{bmatrix} \tag{14}$$

where $\lambda_n \in (0, 1]$, $(\forall n = 2, \cdots, N-1, N)$, $\mathbf{S}_{\lambda\_i}$ is pretreatment lower triangular, $\mathbf{I}$ is identity matrix, and $\mathbf{P}_{\lambda\_i}$ is left multiplied by (11), the result can be obtained as in (15) shown at the bottom of this page.

Then we can apply (13) to obtain the coefficients in multi-band case. The basic iteration form corresponding to (12) is

$$\mathbf{h}_i^{(k+1)} = (\mathbf{A}_i\mathbf{P}_{\lambda\_i})^{-1}\mathbf{B}_i\mathbf{P}_{\lambda\_i}\mathbf{h}_i^{(k)} + (\mathbf{A}_i\mathbf{P}_{\lambda\_i})^{-1}\mathbf{P}_{\lambda\_i}\mathbf{Y}_i \tag{16}$$

Similar methods are used to process other bands to obtain the final full band coefficients. In this way, the extended full-band distortion can be compensated and the linearization performance of the maximum bandwidth range can be obtained.

C. THE NON-OVERLAPPING SITUATIONS

In the case of tri-band in this paper, if the interval between each band is large enough, the intermodulation and harmonic products will be far away from the useful signal and have no influence on the system, because these products can

$$\begin{aligned} \mathbf{X}_{\lambda\_i} &= \mathbf{P}_{\lambda\_i}\mathbf{X}_i = (\mathbf{I} + \mathbf{S}_{\lambda\_i})(\mathbf{I} - \mathbf{L}_i - \mathbf{U}_i) \\ &= \begin{bmatrix} 1 & x_{12} & \cdots & x_{1,N} \\ x_{21} - \lambda_2 x_{21} & 1 - \lambda_2 x_{12}x_{21} & \cdots & x_{2,N} - \lambda_2 x_{1,N}x_{21} \\ \vdots & \vdots & \ddots & \vdots \\ x_{N-1,1} - \lambda_{N-1}x_{N-1,1} & x_{N-1,2} - \lambda_{N-1}x_{12}x_{N-1,1} & \cdots & x_{N-1,N} - \lambda_2 x_{1,N}x_{21} \\ x_{N,1} - \lambda_N x_{N,1} & x_{N,2} - \lambda_N x_{12}x_{N,1} & \cdots & 1 - \lambda_N x_{1,N}x_{N,1} \end{bmatrix} \\ &= \mathbf{D}_\lambda - \mathbf{L}_\lambda - \mathbf{U}_\lambda \end{aligned} \tag{15}$$

be filtered out. However, in traditional methods, harmonic and other distortion components need to meet the following conditions to avoid overlaping [7]. As mentioned above, we define that the angular frequencies of the three bands are ω_1, ω_2, and ω_3 respectively, and $\omega_3 > \omega_2 > \omega_1$. The frequency spacing between band1 and band2 is defined as δ_{12}, and the frequency spacing between band2 and band3 is defined as δ_{23}. It is assumed that the maximum bandwidth of the three bands is W_{max}, and $W_{max} > 0$.

Due to the limitation of transmission bandwidth in a real communication, the frequency interval cannot increase indefinitely. We first explain the phenomenon and cause of spectral aliasing in this section. According to Nyquist's theorem, aliasing occurs obviously when the sampling frequency is less than 2 times the signal bandwidth. After PA amplification, harmonic components, intra-band intermodulation components, intermodulation components and cross-modulation components are generated in the output signal. Some of these components such as $2\omega_1$, $\omega_2 + \omega_1 - \omega_3$, $2\omega_3 - \omega_2$, and $2\omega_2 - \omega_3$ etc in the base band of interest will affect the linearization performance of PA or increase the modeling complexity.

In order to get a complete distortion component from the feedback loop and modeling more accurate, the output bandwidth is often required to reach 5-times the input bandwidth according to the theoretical basis of narrow band system. Therefore, the center frequencies of intermodulation and harmonic products should locate 5-times beyond the range of W_{max} in the center of the three bands. In other words, the combination of the three bands should meet the follwing conditions: $\pm(\beta_1\omega_1 \pm \beta_2\omega_2 \pm \beta_3\omega_3) \notin (\omega_i - 5W_{max},\ \omega_i + 5W_{max})$, $(i = 1, 2, 3)$, where β_1, β_2 and β_3 are the possible combination coefficient of the three bands, and the range of their sum is $2 \leq (\beta_1 + \beta_2 + \beta_3) \leq 5$, $(\beta_1, \beta_2, \beta_3) \in \{0, 1, 2, 3, 4, 5\}$. It also satisfies the relationship $\delta_{12} \geq 5W_{max}$, $\delta_{23} \geq 5W_{max}$, and $\omega_1 > 5W_{max}$.

The coefficients of all possible values ω_i $(i = 1, 2, 3)$ are listed, duplicate and unqualified results are eliminated, as shown in (17). In order to ensure that all lower than 5-order harmonic products and cross-modulation products of tri-band signal away from the basic band, the non-overlapping conditions need to be satisfied, and these distortion components can be removed by the filter.

$$\begin{cases} \delta_{12}, \delta_{23}, \omega_1 \geq 5W_{\max} \\ |r_2\delta_{12} - r_3\delta_{23}| \notin (-5W_{\max}, 5W_{\max}), \\ \quad (r_2, r_3 = 1, 2, r_2 + r_3 \leq 3) \\ \delta_{12}, \delta_{23}, \delta_{12} + \delta_{23}, \delta_{23} - \delta_{12} \\ \notin (r_4\omega_1 - 5W_{\max}, r_4\omega_1 + 5W_{\max}), \quad (1 \leq r_3 \leq 4) \\ \delta_{12} + 2\delta_{23}, 2\delta_{12}, 2\delta_{23}, 2\delta_{12} + \delta_{23}, 2\delta_{12} + 2\delta_{23} \notin \\ (r_4\omega_1 - 5W_{\max}, r_4\omega_1 + 5W_{\max}), \quad (r_4 = 1, 2) \\ \delta_{23} - r_5\delta_{12} \notin (r_6\omega_1 - 5W_{\max}, r_6\omega_1 + 5W_{\max}), \\ 2 \leq r_5 \leq 3, \quad (r_5 - 1) \leq r_6 \leq 4. \\ \delta_{23} - 4\delta_{12} \notin (4\omega_1 - 5W_{\max}, 4\omega_1 + 5W_{\max}) \end{cases} \tag{17}$$

If the system satisfies the condition that the multi-band does not overlap, we can verify whether the given tri-band signal can be properly linearized without considering the harmonic and cross-modulation distortion products. Nevertheless, the system does not meet the non-overlapping conditions, anti-aliasing method should be applied to deal with overlapping phenome-non to avoid serious distortion.

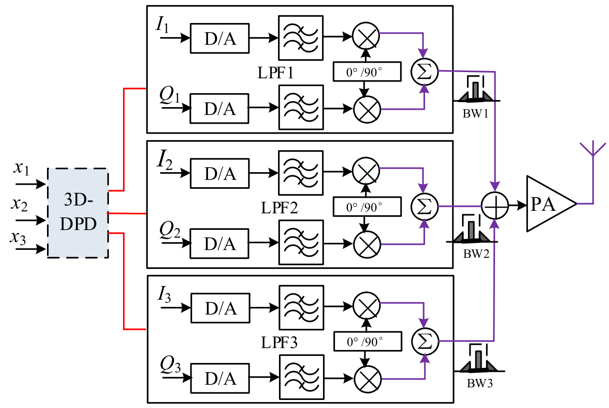

FIGURE 2. Block diagram of tri-band system with I/Q compensation.

D. I/Q COMPENSATION

In order to ensure the signal to be transmitted reliably, the nonlinear distortion and I/Q imbalance generated by the PA must be compensated effectively. Recent studies show that, the combination of two distortion compensation methods is more effective. The block diagram of tri-band system with I/Q compensation is shown in Fig. 2. We suppose the tri-band complex baseband input signals at the three bands are $x_1(t)$, $x_2(t)$, $x_3(t)$, and can be given as $x_i(t) = I_i(t)+jQ_i(t)$, $(i = 1, 2, 3)$, where $I_i(t)$ and $Q_i(t)$ are the in-phase and quadrature components. Then, each signal is modulated to their corresponding RF bands, and the RF bands are ω_1, ω_2, and ω_3 respectively. Signals with orthogonal modulation and up-conversion are shown as

$$\begin{aligned} \tilde{x}_1(t) &= \tilde{I}_1(t)\cos(\omega_1 t) - \tilde{Q}_1(t)\sin(\omega_1 t) \\ &= \lambda_{11}\tilde{I}_1(t)\cos(\omega_1 t + \varphi_{11}) - \lambda_{12}\tilde{Q}_1(t)\sin(\omega_1 t + \varphi_{12}) \end{aligned} \tag{18}$$

$$\begin{aligned} \tilde{x}_2(t) &= \tilde{I}_2(t)\cos(\omega_2 t) - \tilde{Q}_2(t)\sin(\omega_2 t) \\ &= \lambda_{21}\tilde{I}_2(t)\cos(\omega_2 t + \varphi_{21}) - \lambda_{22}\tilde{Q}_2(t)\sin(\omega_2 t + \varphi_{22}) \end{aligned} \tag{19}$$

$$\begin{aligned} \tilde{x}_3(t) &= \tilde{I}_3(t)\cos(\omega_3 t) - \tilde{Q}_3(t)\sin(\omega_3 t) \\ &= \lambda_{31}\tilde{I}_3(t)\cos(\omega_3 t + \varphi_{31}) - \lambda_{32}\tilde{Q}_3(t)\sin(\omega_3 t + \varphi_{32}) \end{aligned} \tag{20}$$

where $\tilde{I}_i(t)$ and $\tilde{Q}_i(t), (i = 1, 2, 3)$ are the in-phase and quadrature components of the input signal which after being modulated and up-converted. If the modulator is ideal, and $\tilde{I}_i(t)$, $\tilde{Q}_i(t)$, $(i = 1, 2, 3)$ satisfy the following relation $\tilde{I}_i(t) = I_i(t)$ and $\tilde{Q}_i(t) = Q_i(t), (i = 1, 2, 3)$. In the actual communication system, however, the I/Q modulators are not ideal, and can be expressed in discrete time as follows.

$$\tilde{I}_i(n) = c_{i1}\cos(\alpha_{i1})I_i(n) - c_{i2}\sin(\alpha_{i2})Q_i(n) \quad (21)$$

$$\tilde{Q}_i(n) = c_{i1}\sin(\alpha_{i1})I_i(n) - c_{i2}\cos(\alpha_{i2})Q_i(n) \quad (22)$$

where c_{i1} and c_{i2} are the parameters related to gain imbalance G_i, $(i = 1, 2, 3)$, and the relationship between them is $c_{i2}/c_{i1} = 10^{(Gi/20)}$. In (21) and (22), α_{i1} and α_{i2} are the parameters related to phase imbalance. The overall broadband input signal $x(t)$ is generated by combining three RF signals, and then it drives the broadband PA, resulting in pass-band output $\tilde{y}_1(t)$, $\tilde{y}_2(t)$ and $\tilde{y}_3(t)$ respectively. Their discrete form of the expressions is shown below:

$$\begin{aligned}\tilde{y}_1(n) = &\sum_{\substack{r=1\\odd}}^{N}\sum_{\substack{d=1\\odd}}^{r}\sum_{q_r=0}^{Q_r} h_{rd}^{(1)}(q_r)\tilde{x}_1(n-q_1)\xi_{r,d,q_r}\\ &\times[\tilde{x}_1(n),\tilde{x}_2(n),\tilde{x}_3(n)]\\ &+\sum_{\substack{r=1\\odd}}^{N}\sum_{\substack{d=1\\odd}}^{r}\sum_{q_r=0}^{Q_r} \tilde{h}_{rd}^{(1)}(q_r)\tilde{x}_1^*(n-q_1)\xi_{r,d,q_r}\\ &\times[\tilde{x}_1(n),\tilde{x}_2(n),\tilde{x}_3(n)]\end{aligned} \quad (23)$$

$$\begin{aligned}\tilde{y}_2(n) = &\sum_{\substack{r=1\\odd}}^{N}\sum_{\substack{d=1\\odd}}^{r}\sum_{q_r=0}^{Q_r} h_{rd}^{(2)}(q_r)\tilde{x}_2(n-q_1)\xi_{r,d,q_r}\\ &\times[\tilde{x}_1(n),\tilde{x}_2(n),\tilde{x}_3(n)]\\ &+\sum_{\substack{r=1\\odd}}^{N}\sum_{\substack{d=1\\odd}}^{r}\sum_{q_r=0}^{Q_r} \tilde{h}_{rd}^{(2)}(q_r)\tilde{x}_2^*(n-q_1)\xi_{r,d,q_r}\\ &\times[\tilde{x}_1(n),\tilde{x}_2(n),\tilde{x}_3(n)]\end{aligned} \quad (24)$$

$$\begin{aligned}\tilde{y}_3(n) = &\sum_{\substack{r=1\\odd}}^{N}\sum_{\substack{d=1\\odd}}^{r}\sum_{q_r=0}^{Q_r} h_{rd}^{(3)}(q_r)\tilde{x}_3(n-q_1)\xi_{r,d,q_r}\\ &\times[\tilde{x}_1(n),\tilde{x}_2(n),\tilde{x}_3(n)]\\ &+\sum_{\substack{r=1\\odd}}^{N}\sum_{\substack{d=1\\odd}}^{r}\sum_{q_r=0}^{Q_r} \tilde{h}_{rd}^{(3)}(q_r)\tilde{x}_3^*(n-q_1)\xi_{r,d,q_r}\\ &\times[\tilde{x}_1(n),\tilde{x}_2(n),\tilde{x}_3(n)]\end{aligned} \quad (25)$$

where $h_{rd}^{(i)}$ are the Volterra model coefficients of PA, ξ_{r,d,q_r} is the score for three input signals, and the expression is

$$\begin{aligned}&\xi_{r,d,q_r}[\tilde{x}_1(n),\tilde{x}_2(n),\tilde{x}_3(n)]\\ &= \prod_{u=1}^{(d-1)/2}\tilde{x}_1(n-q_{2u})\tilde{x}_1^*(n-q_{2u+1})\\ &\quad\times\prod_{u=(d+1)/2}^{(r-d)/2}\tilde{x}_2(n-q_{2u})\tilde{x}_2^*(n-q_{2u+1})\\ &\quad\times\prod_{u=(r-d+1)/2}^{(r+d)/2}\tilde{x}_3(n-q_{2u})\tilde{x}_3^*(n-q_{2u+1})\end{aligned} \quad (26)$$

The final output is shown as

$$\begin{aligned}&y_{\mathrm{I/Q}}(n)\\ &= \sum_{m=0}^{M+L_1} r_1 x(n-m) + \sum_{m=0}^{M+L_2} r_2 x^*(n-m)\\ &\quad+\sum_{\substack{k=1\\k-odd}}^{K_a}\sum_{m=0}^{M_a}\sum_{l=0}^{L_1}\eta_{kml\_1}(x(n))+\sum_{\substack{k=1\\k-odd}}^{K_{a1}}\sum_{m=0}^{M_{a1}}\\ &\quad\times\sum_{l=0}^{L_2}\overline{\eta}_{kml\_1}(x(n))+\sum_{\substack{k=3\\k-odd}}^{K_b}\sum_{m=0}^{M_b}\sum_{q=1}^{Q_b}\sum_{l=0}^{L_1}\eta_{kmql\_2}(x(n))\\ &\quad+\sum_{\substack{k=3\\k-odd}}^{K_{b1}}\sum_{m=0}^{M_{b1}}\sum_{q=1}^{Q_{b1}}\sum_{l=0}^{L_2}\overline{\eta}_{kmql\_2}(x(n))\\ &\quad+\sum_{\substack{k=3\\k-odd}}^{K_c}\sum_{m=0}^{M_c}\sum_{q=1}^{Q_c}\sum_{l=0}^{L_1}\eta_{kmql\_3}(x(n))\\ &\quad+\sum_{\substack{k=3\\k-odd}}^{K_{c1}}\sum_{m=0}^{M_{c1}}\sum_{q=1}^{Q_{c1}}\sum_{l=0}^{L_2}\overline{\eta}_{kmql\_3}(x(n))\end{aligned} \quad (27)$$

In the case of tri-band, the computational complexity is increased with the further expansion of the model to characterize the cross-modulation effect. As shown in (27), the I/Q is devoted to compensate for the I/Q impairments generated in the two quadrature modulator tri-band behavioral model. Since each band signal needs to be transmitted to the channel through a separate I/Q modulator, the serious distortion caused by I/Q imbalance can be amplified in a multi-band system. I/Q defect of the concurrent multi-band transmitter is much greater than that of the single-band transmitter. Therefore, compensation for I/Q imbalance is more important in multi-band systems.

IV. EXPERIMENTAL ENVIRONMENT AND LINEARIZATION

A. MULTI-BAND EXPERIMENTAL CONDITIONS

In this section, several tri-band scenarios with different frequency spacing are tested, and extensive band algorithm is assessed and compared with the conventional methods. In the first experiment, the device under test used for model validation is a class-F wideband PA. The peak output power of the PA is 30W, the compression point power of 1 dB at saturated output is $P_{1dB} = 44$dBm, $V_{ds} = 28$V, $V_{gs} = -5$V, and the frequency range is from 1.0 GHz to 3.0 GHz. The test bench is set up to be similar to that in [8]. The transmitter and feedback path apply indirect RF learning structure. All the necessary calculations and algorithms before digital-to-analog converter (DAC) and after ADC are carried out on the host personal computer (PC) by Matlab. In the binomial expansion of the tri-band input and output system, only the three fundamental frequencies (ω_1, ω_2, and ω_3) of input signal are set up for 3-D predistortion model, because other frequency components are far away from the effective signal and can be filtered. The frequency of each baseband signal is converted up to the corresponding RF frequency and then combined with a broadband synthesizer to send to PA. The output signal is captured by the vector signal analyzer (VSA) and the whole spectrum is obtained. In order to establish the amplifier behavior model, the three bands should be collected respectively. The signal is acquired in three steps, and each step corresponds to a frequency band.

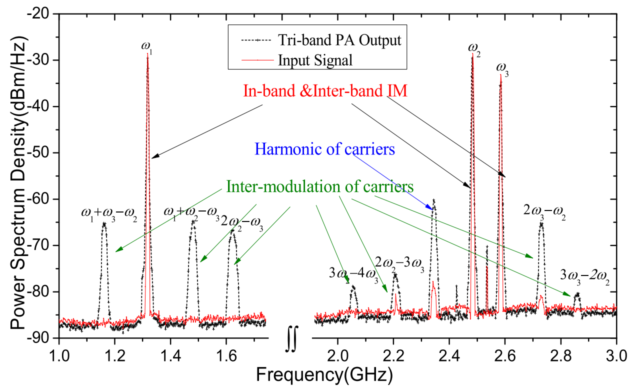

FIGURE 3. Measured spectrum of tri-band input and output signal.

In actual broadband communication, the frequency interval of the transmitted signal cannot be extended indefinitely due to the limited bandwidth of the transmitter. The center frequencies of the tri-band signal are set as $\omega_1 = 1310$ MHz, $\omega_2 = 2490$ MHz, and $\omega_3 = 2580$ MHz. After the tri-band input signal passes through the PA, its power spectral density (PSD) is tested at the output ends, and the results are shown in Fig. 3. It can be seen from the results that the output signal not only contains three base-band frequency products, but also inter-modulation products, in-band inter-modulation products, and cross-modulation products. In particular, the components closer to the base band frequency cannot be ignored in the modeling, because these products are high enough to affect the effective signal. If the bandwidth of ω_2 is 30 MHz, the 5-th order inter-harmonic cross modulation product will be covered in the middle band from 2445 MHz to 2530 MHz. Especially the spectrum extension on the right has entered near the primary frequency range of the third band $\omega_3 = 2595$ MHz, which will affect its performance seriously.

The general non-overlapping condition of tri-band signal is an important contribution in this paper. It is significant to model the behavior of multi-band in discontinuous CA system.

The constituent of the tri-band signals are 20 MHz LTE signal at 1.31 GHz, a 20 MHz 4-carrier wideband code division multiple access (WCDMA) signal at 2.49 GHz, and a 20 MHz 2-carrier WiMAX signal at 2.58 GHz respectively. The three signals are sent concurrently, and are operated at sampling frequency of 368.64 Msps. The scanning range of VSA is set to 200 MHz around each frequency band. The input and output baseband signals of each frequency band should be processed synchronously to obtain an accurate model. The memory depth and nonlinear order are set to $M = 5$ and

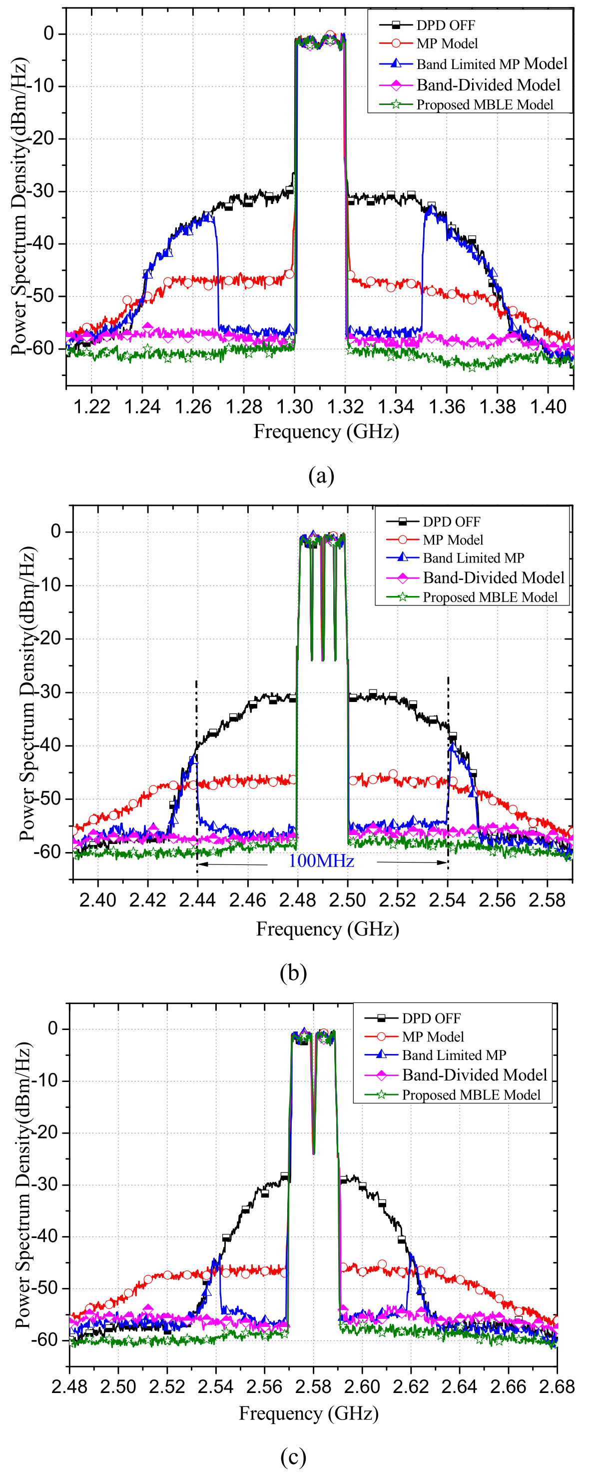

FIGURE 4. Measured output spectrum with proposed MBLE model and conventional method under different center frequency (a) 1.31 GHz (b) 2.49 GHz (c) 2.58 GHz.

$K = 7$ respectively, and DPD coefficients are extracted by least square (LS) method.

B. PRE-DISTORTION EFFECT OF RECEPTION SIGNAL

PSDs around the three bands are tested, and the spectrums obtained under different methods are compared. The results are shown in Fig. 4. In this experiment, the pre-distortion effects of memory polynomial (MP) model, band limited MP (BL-MP) model, band divided (BD) model and proposed MBLE model are compared. The parameters of memory depth and nonlinear order of these models are set to $M_{MP} = 5$, $K_{MP} = 9$, $M_{BL-MP} = 7$, $K_{BL-MP} = 9$, $M_{BD} = 5$, $K_{MD} = 7$, $M_{MBLE} = 5$, $K_{MBLE} = 7$, respectively. In the feedback loop, we use cavity bandpass filters in the 80MHz and 100MHz passband ranges to limit the signal bandwidth, and each filter can operate at the corresponding central frequency. Fig. 4 (a) is the spectrum result of the central frequency at 1.31 GHz. It can be obtained from the analysis of the figure that the distortion is significantly relief after DPD being introduced.

Compared to the pre-distortion effects of several different models, we note that MP model has very little improvement, because the model bandwidth does not match the actual bandwidth, resulting in low modeling accuracy. BL-MP model only gets better effect in the band limited frequency range, and deteriorates rapidly outside the band limited area. The proposed MBLE model can suppress distortion well in the whole frequency band. ACPR is 14 dB better than MP model, and 4dB better than BD model while no complexity increases.

Fig. 4 (b) shows the spectrum test results of the 4-carrier WCDMA signal with the center frequency at 2.49 GHz. Similarly, the proposed MBLE model has effectively suppressed the spectral distortion in the adjacent channels. Fig. 4 (c) shows the spectrum results of 2-carrier WiMAX signal in the third frequency band at the central frequency 2.58 GHz, the results are similar to Fig. 4 (a) and (b). The signal bandwidths of the three bands are all 20 MHz, the sampling rate of the proposed MBLE model is 76.8 MSPS, and Nyquist bandwidth is 30.72 MHz. The sampling rate of MP model is 184.32 MSPS, the sampling rate of BD model is 122.88 MSPS.

C. THE RESULTS OF NMSE AND EVM

According to the tri-band limited and I/Q compensation model given in (27), the nonlinear order and memory depth are set as $K_a = 9$, $K_b = 7$, $K_c = 5$, $K_{a1} = 9$, $K_{b1} = 7$, $K_{c1} = 7$, M_a, M_b and M_c are all set to 5, $L_1 = 5$, $L_2 = 3$ respectively. The model accuracy of the proposed method is measured by the normalized mean square error (NMSE) [23], the calculation expression of NMSE is shown in (28).

$$\mathrm{NMSE}_i = 10\log_{10}\left(\frac{\sum_{n=1}^{N} |y^i_{\mathrm{meas}}(n) - y^i_{\mathrm{est}}(n)|^2}{\sum_{n=1}^{N} |y^i_{\mathrm{meas}}(n)|^2}\right) \tag{28}$$

where $y^i_{\mathrm{meas}}(n)$ is the actual measurement output of signal, $y^i_{\mathrm{est}}(n)$ is the estimated output of the behavior model, ($i = 1, 2, 3$) is used to mark low band, medium band and high band, N is the number of elements. The test results of NMSE are shown in Fig 5.

It can be seen that with the increase of bandwidth, the NMSE of the three bands reaches their optimum.

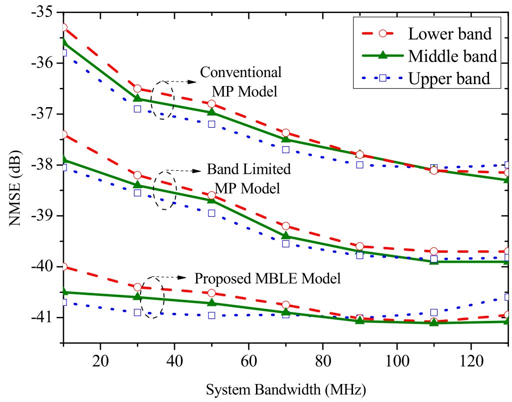

FIGURE 5. Modeling NMSEs versus system bandwidth.

However, when the acquisition bandwidth is relatively narrow (less than 20 MHz), the performance of the MP model and band limited model deteriorates significantly. The NMSE values obtained by the proposed MBLE method are relatively stable, because band limited spread model and I/Q compensation are combined employed and it can get high accuracy less than −41dB. Even if the bandwidth is less than 20MHz, NMSE still reaches about −40 dB.

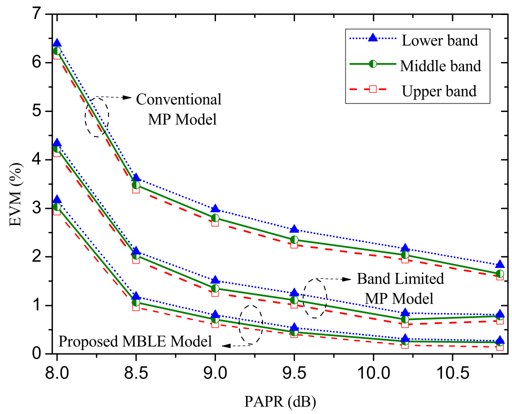

FIGURE 6. Comparison of EVM among different methods.

Error vector magnitude (EVM) can be used to evaluate the in-band performance of the compensation algorithm. EVM is the vector difference between the ideal reference signal and the actual signal sent at a given time, including the amplitude error and phase error. The calculation formula of EVM is shown in (29), which is expressed as a percentage. Where S is the actual measurement vector of the signal, R is the reference vector, and RMS (∗) represents the root mean square value. The test results of EVM are shown in Fig. 6.

$$\mathrm{EVM} = \frac{\mathrm{RMS}(|S - R|)}{\mathrm{RMS}(|R|)} \times 100\% \tag{29}$$

Fig. 6 shows the EVM with different carriers iterating off-line. In the DPD model, the performance is improved by adapting to the device changes caused by different excitation signals. The triangular symbol represents the EVM performance of lower band, the circular symbol represents the result of middle band, and the square shape represents the result of upper band. The modulation mode adopted in the experimental test is 16 quadrature amplitude modulation (16QAM). It can be seen that the EVM performance of the proposed MBLE model is optimistic obviously. It is 1% better than BL-MP model and 2.3% better than conventional MP model when PAPR is 9dB.

We applied multi-band crest factor reduction (CFR) technology to reduce PAPR [24]. Input signals are defined as above, and S is defined as the peak clipping threshold. For the case of tri-band signals, peak clipping signal can be achieved by the following equation

If $|x_1(n)| + |x_2(n)| + |x_3(n)| > S$, then

$$\begin{aligned} |\widetilde{x}_{1,\text{clipped}}(n)| &= \frac{|\widetilde{x}_1(n)|}{|\widetilde{x}_1(n)| + |\widetilde{x}_2(n)| + |\widetilde{x}_3(n)|} \cdot S \\ |\widetilde{x}_{2,\text{clipped}}(n)| &= \frac{|\widetilde{x}_2(n)|}{|\widetilde{x}_1(n)| + |\widetilde{x}_2(n)| + |\widetilde{x}_3(n)|} \cdot S \\ |\widetilde{x}_{3,\text{clipped}}(n)| &= \frac{|\widetilde{x}_3(n)|}{|\widetilde{x}_1(n)| + |\widetilde{x}_2(n)| + |\widetilde{x}_3(n)|} \cdot S \end{aligned} \tag{30}$$

where $\widetilde{x}_{i,\text{clipped}}(n)$ $(i = 1, 2, 3)$ are peak clipping signals, PAPR was reduced from 11.3 dB to 9 dB by clipping with CFR technology. There was a small increase in EVM (about 0.6%) after peak clipping, but the study showed that this did not affect the overall performance.

V. SYSTEM EXPERIMENTAL CHARACTERISTICS

A. SIGNAL NON-ALIASING AND THE EFFECTS

In order to verify the spectral characteristics of several methods under the condition of non-overlapping signals, a 40W GaN Doherty amplifier ($V_{ds} = 28V$, $V_{gs} = -2.7V$) is tested in this section, and the results are shown in Fig. 7. The test results before and after DPD in three cases were displayed, and only case 3 satisfy the condition of no aliasing. The signal bandwidth of each band is set at 30 MHz, and the spectral results of the lower/middle/upper band are respectively observed, which are shown as the '0' frequency here.

As shown in Fig. 7, excellent suppression effect is obtained under the condition of non-overlapping bandwidth. However, linearization performance deteriorated prominently and significantly asymmetric under the condition of does not satisfy the non-superposition. This is because the cross-modulation and inter-modulation components are mixed together and are not effectively inhibited, PSD performance will decline by about 10 dB. Case 1 and case 2 are also tested and illustrated as important comparisons. Generally, the signal spacing is set to satisfy the non-aliasing condition. Although aliasing may causes serious distortion, we can also adopt some methods to reduce the influence of distortion.

B. I/Q COMPENSATION AND AMPLITUDE CHARACTERISTICS

In view of the existence of I/Q imbalance, this paper proposed a multi-band I/Q compensation method, and ascendant compensation effect is obtained. The comparative analysis

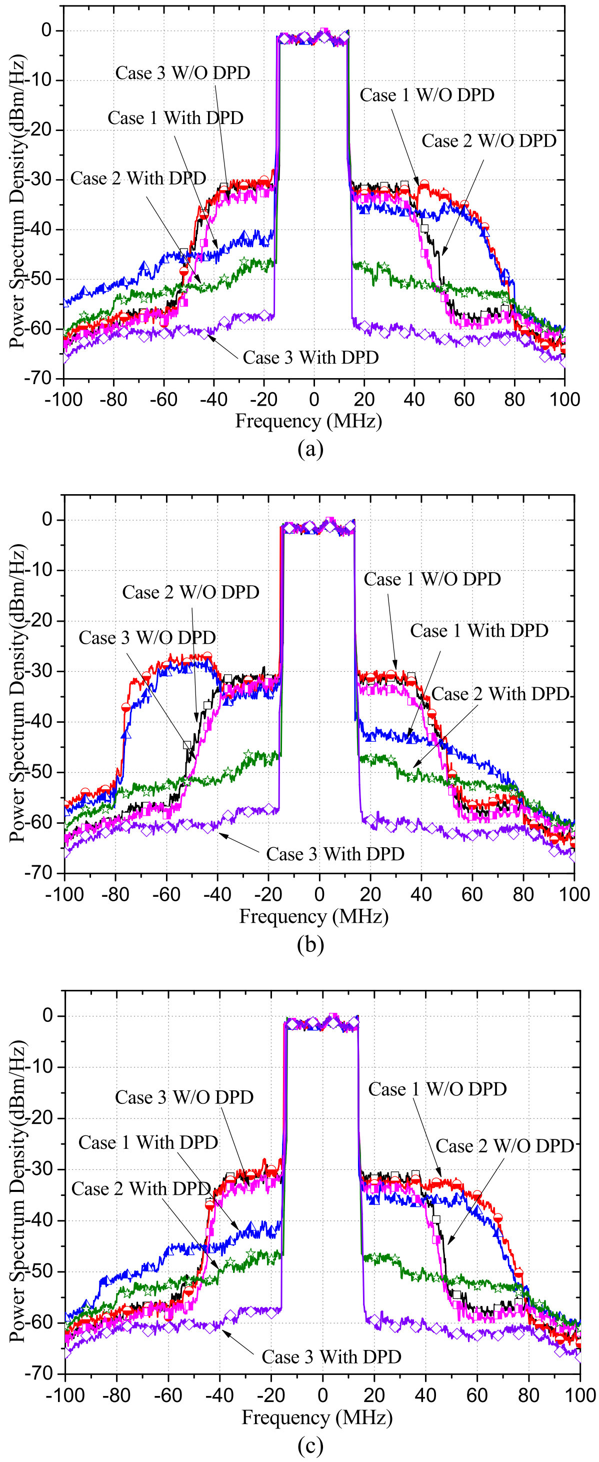

FIGURE 7. Measured output spectra with different frequency spacing. (a) Lower band (b) Middle band (c) Upper band.

results of I/Q compensation and pre-distortion performance are shown in Table I. The results of various parameters before and after DPD were analyzed. The predistortion performance of the traditional and proposed method was compared in detail. It can be seen that there is no significant change of the output power before and after predistortion. With the improvement of model precision, the number of model series

TABLE 1. Comparison of output power, NMSE and ACPR for tri-band signals with different spacing.

DPD Mthods	Output Power (dBm)	NMSE (dB)	Number of Coefficients	ACPR@ -/+10MHz (dBc)
Without DPD	35	-29.54	N/A	-34.21/-35.49
MP DPD	32	-36.32	98	-51.35/-52.28
BD DPD	34	-38.67	240	-55.45/-56.12
MBLE DPD	36	-40.52	145	-60.58/-59.77

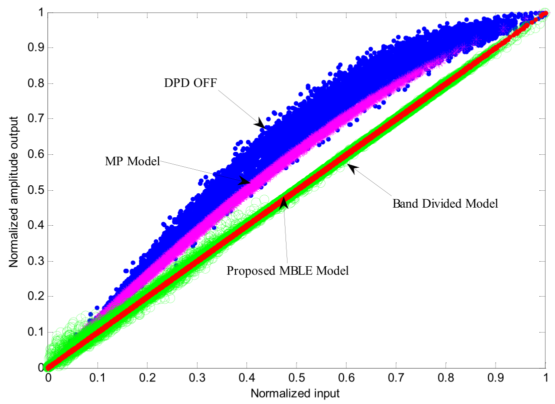

FIGURE 8. Measured AM/AM characteristics of the DUT.

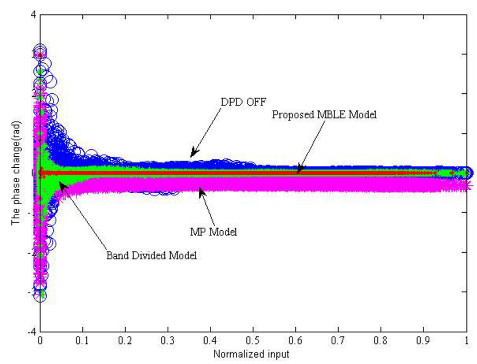

FIGURE 9. Measured AM/PM characteristics of the DUT.

decreases, the number of coefficients was reduced by 95 relative to the BD model. The value of ACPR, which represents the linearization performance, was also improved by 4.39dB.

The Amplitude/Amplitude modulation (AM/AM) and Amplitude/Phase modulation (AM/PM) characteristics represent the magnitude and the phase of the instantaneous gain measured using the modulated test signal. AM/AM and AM/PM are used to qualitatively characterize the input and output characteristics of the PA and its model. The characteristics of the power amplifier under test are shown in Fig. 8 and Fig. 9 respectively. Due to the inherent nonlinear and memory effects of PA, significant dispersion exists in the AM/AM and AM/PM characteristics for low input power levels. The dispersion is reduced as the input power level increases, and with the introduction of predistorter, the nonlinear and memory effects decrease obviously. AM/AM is close to linear relationship and there is almost no phase offset applied the proposed MBLE method.

VI. CONCLUSION

A new sampling rate reduction and I/Q imbalanced compensation method for tri-band or multi-band predistortion systems are proposed. This paper discusses that the tri-band predistortion is limited by the sampling rate of the feedback loop and puts forward higher requirements for the system. I/Q up-converter with low sampling rate is adopted to verify the I/Q imbalanced and nonlinear distortion compensation method of 1-3 GHz intermodulation multiband signals. The proposed algorithm is applied to preprocess the input signal which is formed by a 20 MHz LTE signal at 1.31 GHz, a 20 MHz 4-carrier WCDMA signal at 2.49 GHz, and a 20 MHz 2-carrier WiMAX signal at 2.58 GHz respectively. Then the processed signal was used to drive a broadband PA. The experimental results show that the proposed method can successfully establish DPD model under the condition of insufficient sampling, and improve the performance of multi-band systems significantly, and is more cost effective.

ACKNOWLEDGMENT

The authors would like to thank the anonymous reviewers for their constructive comments which helped them improve the quality and presentation of this article.

REFERENCES

[1] S. A. Bassam, M. Helaoui, and F. M. Ghannouchi, "2-D digital predistortion (2-D-DPD) architecture for concurrent dual band transmitters," *IEEE Trans. Microw. Theory Techn.*, vol. 59, no. 10, pp. 2547–2554, Oct. 2011.

[2] X. Liu, Q. Zhang, W. Chen, H. Feng, L. Chen, F. M. Ghannouchi, and Z. Feng, "Beam-oriented digital predistortion for 5G massive MIMO hybrid beamforming transmitters," *IEEE Trans. Microw. Theory Techn.*, vol. 66, no. 7, pp. 3419–3432, Jul. 2016.

[3] S.-H. Li, S. H. S. Hsu, J. Zhang, and K.-C. Huang, "Design of a Compact GaN MMIC Doherty power amplifier and system level analysis with X-parameters for 5G communications," *IEEE Trans. Microw. Theory Techn.*, vol. 66, no. 12, pp. 5676–5684, Dec. 2018.

[4] K. Gumber and M. Rawat, "Low-Cost RF_{in}–RF_{out} predistorter linearizer for high-power amplifiers and ultra-wideband signals," *IEEE Trans. Instrum. Meas.*, vol. 67, no. 9, pp. 2069–2081, Sep. 2018.

[5] M. Abdelaziz, L. Anttila, C. Tarver, K. Li, J. R. Cavallaro, and M. Valkama, "Low-complexity subband digital predistortion for spurious emission suppression in noncontiguous spectrum access," *IEEE Trans. Microw. Theory Techn.*, vol. 64, no. 11, pp. 3501–3517, Nov. 2016.

[6] C. Yu, N. Yang, H. Sun, X. Wu, J. Zhai, and X. Zhu, "Near-band digital predistortion for wideband power amplifiers with mmWave non-contiguous carrier aggregation," *IEEE Electron. Lett*, vol. 53, no. 20, pp. 1366–1368, Sep. 2017.

[7] C. Yu and Z. Zhang, "Non-overlapping conditions to enable multi-dimensional behavioral models/DPDs for multi-band or non-continuous carrier aggregation systems," *China Commun.*, vol. 14, no. 2, pp. 30–39, Feb. 2017.

[8] M. Younes, A. Kwan, M. Rawat, and F. M. Ghannouchi, "Three-dimensional digital predistorter for concurrent tri-band power amplifier linearization," in *IEEE MTT-S Int. Microw. Symp. Dig.*, Jun. 2013, pp. 1–4.

[9] T. Tian, Y. Zhao, Y. Dou, C. Yu, and J. Qiu, "A novel concurrent tri-band digital predistortion for broadband signals," in *Proc. Eur. Microw Conf. (EuMC)*, Paris, France, 2015, pp. 1136–1139.

[10] G. Su and W. Chen, "Digital predistortion for concurrent multi-band PAS with inter-band IMD compensation," *IEEE Electron. Lett*, vol. 49, no. 18, pp. 1163–1165, Aug. 2016.

[11] E. Zenteno and D. Rönnow, "MIMO subband volterra digital predistortion for concurrent aggregated carrier communication," *IEEE Trans. Microw. Theory Techn.*, vol. 65, no. 3, pp. 967–979, Mar. 2017.

[12] C. Yu, L. Guan, E. Zhu, and A. Zhu, "Band-limited volterra series-based digital predistortion for wideband RF power amplifiers," *IEEE Trans. Microw. Theory Techn.*, vol. 60, no. 12, pp. 4198–4208, Dec. 2012.

[13] C. Yu, M. A. Martínez, Y. Guo, and A. Zhu, "Output-controllable partial inverse digital predistortion for RF power amplifiers," *IEEE Trans. Microw. Theory Techn.*, vol. 62, no. 11, pp. 2499–2510, Nov. 2014.

[14] F. Mkadem, A. Islam, and S. Boumaiza, "Multi-band complexity-reduced generalized memory-polynomial power-amplifier digital predistortion," *IEEE Trans. Microw. Theory Techn.*, vol. 64, no. 6, pp. 1763–1774, Jun. 2016.

[15] N. Guan, N. Wu, and H. Wang, "Digital predistortion of wideband power amplifier with single undersampling ADC," *IEEE Microw. Wireless Compon. Lett.*, vol. 27, no. 11, pp. 1016–1018, Nov. 2017.

[16] J. Luo, A. Kortke, W. Keusgen, and M. Valkama, "Efficient estimation and pilot-free online re-calibration of I/Q imbalance in broadband direct-conversion transmitters," *IEEE Trans. Veh. Technol.*, vol. 63, no. 6, pp. 2506–2520, Jul. 2014.

[17] A. Chung, M. B. Rejeb, Y. Beltagy, A. M. Darwish, H. A. Hung, and S. Boumaiza, "IQ imbalance compensation and digital predistortion for millimeter-wave transmitters using reduced sampling rate observations," *IEEE Trans. Microw. Theory Techn.*, vol. 66, no. 7, pp. 3433–3442, Jul. 2018.

[18] P. Jaraut, M. Rawat, and F. M. Ghannouchi, "Composite neural network digital predistortion model for joint mitigation of crosstalk, I/Q imbalance, nonlinearity in MIMO transmitters," *IEEE Trans. Microw. Theory Techn.*, vol. 66, no. 11, pp. 5011–5020, Nov. 2018.

[19] K. S. Lorenz, J. Goodman, G. Stantchev, and N. A. Pendergrass, "Generalized transmitter compensation of frequency dependent I/Q imbalance," *IEEE Trans. Signal Process.*, vol. 64, no. 9, pp. 2220–2231, May 2016.

[20] A. Nassery, S. Byregowda, S. Ozev, M. Verhelst, and M. Slamani, "Built-in self-test of transmitter I/Q mismatch and nonlinearity using self-mixing envelope detector," *IEEE Trans. Very Large Scale Integr. (VLSI) Syst.*, vol. 23, no. 2, pp. 331–341, Feb. 2015.

[21] H. Gandhi and W. Abbott, "A digital signal processing solution for PA linearization and RF impairment correction for multi-standard wireless transceiver systems," in *Proc. 40th Eur. Microw. Conf.*, Sep. 2010, pp. 719–722.

[22] Z. A. Khan, E. Zenteno, P. Händel, and M. Isaksson, "Digital predistortion for joint mitigation of I/Q imbalance and MIMO power amplifier distortion," *IEEE Trans. Microw. Theory Techn.*, vol. 65, no. 1, pp. 322–333, Jan. 2017.

[23] M. Isaksson, D. Wisell, and D. Ronnow, "A comparative analysis of behavioral models for RF power amplifiers," *IEEE Trans. Microw. Theory Techn.*, vol. 54, no. 1, pp. 348–359, Jan. 2006.

[24] B. Fehri, S. Boumaiza, and E. Sich, "Crest factor reduction of inter-band multi-standard carrier aggregated signals," *IEEE Trans. Microw. Theory Techn.*, vol. 62, no. 12, pp. 3286–3297, Dec. 2014.

JINGMEI ZHAO received the B.S. degree in electronic information science and technology from Liaocheng University, in 2007, and the M.S. degree from Liaoning Technical University, in 2010, and the Ph.D. degree in electronic science and technology from the Beijing University of Posts and Telecommunications, in 2017. She worked as a Researcher, from 2010 to 2013. She is currently an Instructor with the School of Information Science and Engineering, Shandong Normal University. Her current research interests include power amplifier linearization, microwave wireless communication, and distributed network optimization.

LINBO ZHAI received the B.S. and M.S. degrees from the School of Information Science and Engineering, Shandong University, in 2004 and 2007, respectively, and the Ph.D. degree from the School of Electronic Engineering, Beijing University of Posts and Telecommunications, in 2010. Since, he has been a Teacher with Shandong Normal University. His current research interests include cognitive radio, crowdsourcing, and distributed network optimization.

FENG YANG received the B.S. and M.S. degrees in radio electronics from Shandong University, in 1985 and 1988, respectively. He is currently a Professor with the School of Information Science and Engineering, Shandong Normal University, and the Director of the Department of Communication Engineering. He has published more than 30 articles, edited textbooks and edited five books, obtained seven national invention patents, four utility model patents, participated in one national fund project. He has presided over five provincial and university-level education reform projects. He was a recipient of the One Provincial-Level Teaching Achievement Award, the one School-Level Teaching Achievement Award, and three provincial awards for scientific and technological progress.